

Postgrowth Control of the Quantum-Well Band Edge for the Monolithic Integration of Widely Tunable Lasers and Electroabsorption Modulators

Erik J. Skogen, *Student Member, IEEE*, James W. Raring, Jonathon S. Barton, Steven P. DenBaars, and Larry A. Coldren, *Fellow, IEEE*

Abstract— We describe a quantum well intermixing process for the monolithic integration of various devices, each with a unique band edge. The process involves a single ion implant followed by multiple etch and anneal cycles. We have applied this method to design and fabricate widely-tunable sampled-grating DBR lasers with integrated electroabsorption modulators. The devices employ three unique band edges, and demonstrate exceptional tuning, gain, and absorption characteristics.

Index Terms-- Ion implantation, Laser tuning, Semiconductor lasers, Wavelength division multiplexing.

I. INTRODUCTION

Monolithic integration of widely-tunable lasers with supplementary optoelectronic components offer cost reduction, improved performance, and added functionality over existing fixed wavelength components used in optical networks. The sampled-grating (SG) distributed Bragg reflector (DBR) laser is ideal for this purpose, as the lithographically defined mirrors allow for the manipulation of light on chip. The difficulty arises when optimization requires each of the integrated components to possess a unique band edge. Limited by the one-dimensional growth platform used to produce the epitaxial material, the push for monolithic-integration has lead to either compromises in device design or complex processing to achieve the goals.

The solution is the development of a manufacturable wafer-scale process, which allows for the precise control of the band edge across the wafer. In this paper, we describe a process, and present device results using QWI to tune the band edge of the quantum well (QW) active region across the wafer achieving multiple unique QW band edges to fabricate widely-tunable SG-DBR lasers with integrated electroabsorption modulators (EAM).

There are a few general guidelines to bear in mind when implementing a method for monolithic integration. First, the method used should not be prohibitively time consuming or

expensive. This is the key to realizing the cost reduction over existing discrete components. Second, the integration should not lead to device compromises. This is a difficult task due to the fact that each discrete device was designed with a single function in mind and therefore the device structure evolved on an individual basis. However the integrated component must only perform as intended, it does not necessarily need to match the performance of a discrete device. This affords some flexibility in the design of the device in terms of the device structure, possibly allowing devices with differing functionalities to be fabricated using the same growth and processing platform. Lastly, the process complexity should remain constant as the number of integrated components increases. An additional processing step or the substitution of one step for one that is more complex can increase the manufacturing cost and, in the case of complex processing/growth can lead to yield reduction.

There has been some great success in producing simple photonic integrated circuits (PICs) based on various methods. Such methods include but are not limited to butt-joint regrowth [1], selective area growth (SAG) [2], and the use of offset QWs [3]. The first, butt-joint regrowth involves the selective removal of waveguide core material followed by the regrowth of an alternate waveguide core using different material composition. This process is inherently difficult involving a precise etch of the original waveguide core, followed by a regrowth of waveguide material with composition and thickness variables.

Another process, the SAG process, involves selective growth using a mask. In this process a mask is patterned on the surface of the wafer prior to epitaxial growth. The geometry of the mask has a role in determining the growth near the vicinity of the mask and can be used to obtain different compositions and thickness across the wafer. This method is useful in fabricating several band edges across the wafer, but due to the fact that the thickness changes for each of these regions, the optical confinement factor is not at an optimal level in each section.

The use of offset QWs, where the QWs are situated above the waveguide and selectively removed in various regions, has been used with great success in fabricating various integrated structures [3, 4, 5, 6]. However, the use of offset QWs limits the devices to one of two band edges, not allowing for the flexibility necessary for the fabrication of complex PICs. Furthermore, the vary nature of the offset QW design does not allow for the optimal optical mode overlap with the QWs,

Manuscript received February 14, 2003.; revised July 22, 2003.

E. J. Skogen and L. A. Coldren are with the Electrical and Computer Engineering Department, University of California, Santa Barbara, Santa Barbara, CA 93016 USA (e-mail: Skogen@engineering.ucsb.edu).

J. W. Raring, J. S. Barton, and S. P. DenBaars are with the Materials Department, University of California, Santa Barbara, Santa Barbara, CA 93106 USA.

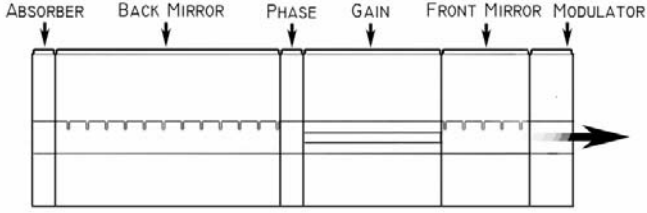


Fig. 1. Schematic cross section of SG-DBR device with integrated EAM. Indicated are the sections of the SG-DBR/EAM device.

leading to a modal gain which is not at the optimal level as compared to a centered QW design.

These methods work very well in producing simple PICs, generally containing fewer than three band edges, but are not well suited for larger scale integration. Large-scale integration requires multiple band edges, ideally one for each integrated component. QWI allows for the strategic, post growth, tuning of the QW band edge in a relatively simple procedure. Here, we employ ion-implantation-induced-intermixing, in which the transition region between sections with differing band edges is predicted to be on the order of a micron [7]. Also, because QWI does not change the average composition, but only slightly changes the compositional profile, there is a negligible index discontinuity at the interface between adjacent sections. This eliminates parasitic reflections that can degrade performance. Our method allows any number of band edges, limited only by the practical number of etch and anneal cycles.

In our case, each section of the SG-DBR laser should be designed with band edges specific to the function of the particular section. This QWI process allows for the as-grown active region to be shifted precise amounts in each section of the PIC, for instance the QW band edge in the mirror and phase sections are blue-shifted to achieve low propagation loss while attaining high tuning efficiency [8], and the QW band edge in the modulator section is blue-shifted to such an extent that a reasonable extinction ratio can be achieved while preserving a low insertion loss.

II. BACKGROUND

A. SG-DBR Background

The general layout for the device is shown in Fig. 1. As shown in the figure, the devices consist of a gain medium with modulated reflectors on either side. A phase section is used to align the cavity mode with the reflectivity peak. The mirrors consist of a modulated grating yielding a comb-like reflectivity spectrum. The peak reflectivity spacing of the front and back mirrors are designed such that only one set reflectivity peaks are aligned at any point within the desired tuning range. The position of the reflectivity peaks can be controlled using carrier injection, producing a shift the absorption edge, leading to a negative change in the refractive index. Therefore, using a relatively small tuning current in one of the mirrors, the adjacent set of reflectivity peaks can be aligned. This is commonly referred to as Vernier effect tuning, and can be exploited to achieve a large tuning range.

A detailed explanation of the operation of the SG-DBR device can be found in [9].

B. EAM Background

In an EAM a reverse electrical bias is used to shift the band edge of the modulator section to lower energy, thereby increasing the absorption of that region. In our case, QWI only smears the interfaces between the QWs and barriers, such that the QWs remain after the intermixing, although shallower and rounded. This allows for the exploitation of the quantum confined Stark effect in the EAM. The rounded shape of the intermixed QW also contributes to increased absorption efficiency in the modulator [10].

III. EXPERIMENT

The focus of this work is development of a quantum well intermixing process that facilitates the formation of a number of unique band edges across the wafer for the monolithic integration of the SG-DBR laser and EAM; where the goals are high output power, good SMSR, wide tunability, and good extinction characteristics. The development of a centered QW active region was a major driving force behind this work. The implementation of an active region with an optimized modal overlap can have far reaching effects on device performance. Nearly all these effects are desirable for achieving optimal performance from the SG-DBR laser and EAM.

As stated earlier, the SG-DBR laser has traditionally made use of offset QWs, where the QWs are situated above the waveguide [3]. In this configuration, the optical mode overlap with the QWs is not at an optimal level. By definition, the modal gain also is not at an optimal level. One of the goals of this work was to improve the optical mode overlap by placing the QWs in the center of the waveguide. By doing so, the optical mode overlap can be optimized, leading to an increased modal gain. Numerical solutions of the optical mode predict that the modal gain is improved by a factor of 1.5 for the centered seven QW design. The improvement in the modal gain allows for the manipulative improvement of observable laser characteristics such as the threshold current, differential efficiency, and output power.

The modal loss of the optically passive regions found in the SG-DBR mirrors and phase sections varies with the extent of intermixing due to the tail of the band edge. This suggests that maximizing the extent of intermixing in the mirror and phase sections will minimize the modal loss in those sections. While minimizing the modal loss in those regions will improve certain laser characteristics, other performance criteria may suffer. In order to study the effects of the placement of the band edge in the mirror and phase sections, several sets of SG-DBR lasers were fabricated with various amounts of intermixing applied to the mirror and phase sections. The number of QWs in the active region is another parameter that has effects on the modal loss, tuning efficiency, and absorption characteristics. Therefore, two epitaxial base structures were grown containing either seven or ten QWs.

Intermixing in the EAM section was carried out such that the QW band edge was intermediate with respect to the gain and mirror sections. In this case the band gap was placed at

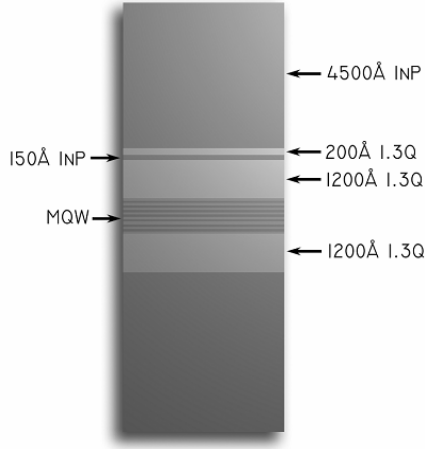


Fig. 2. Epitaxial base structure with both seven- or ten-QW active region, and 4500Å InP implant buffer layer.

around 1500 nm as measured by photoluminescence. This will facilitate a modulator with good extinction characteristics while maintaining reasonable insertion loss. The absorption and bandwidth characteristics for the modulators using intermixed QWs is studied for both seven and ten QW structures as well as for several lengths ranging from 125 μm to 225 μm .

IV. PROCESS

The epitaxial base structure, shown in Fig. 2, was grown on a sulfur doped InP substrate using a Thomas Swan horizontal-flow rotating-disc metal-organic chemical vapor deposition (MOCVD) reactor. Low toxicity metal-organic precursors tertiarybutylarsine (TBA), and tertiarybutylphosphine (TBP) were employed for the group-V sources in our MOCVD process. The active region consists of either seven or ten InGaAsP 7.0 nm compressively strained (1.3%) QWs, separated by 8.0 nm InGaAsP tensile strained (0.3%) barriers, centered within two quaternary InGaAsP waveguide layers with bandgap wavelength of 1.3 μm (1.3Q) designed to optimize the optical mode overlap with the QWs. Following the active region, a 15 nm InP stop etch, a 20 nm 1.3Q stop etch, and a 450 nm InP implant buffer layer was grown.

The active regions were masked with 500 nm of Si_xN_y , and an ion implant was carried out using P^+ at an energy of 100 keV, yielding a range of 90 nm, with a dose of $5\text{E}14 \text{ cm}^{-2}$, at a substrate temperature of 200 $^\circ\text{C}$ [10]. The implant buffer layer was designed to completely capture the ion implant, creating vacancies far from the active region. These vacancies were then partially diffused through the structure during a 90-second, 675 $^\circ\text{C}$ rapid thermal anneal (RTA), yielding the desired band-edge for the EAM. The implant buffer layer above the EAM sections was removed using a wet etching process, stopping on the 1.3Q stop etch layer. The sample was then subjected to an additional 110-second rapid thermal anneal, blue-shifting the regions where the implant buffer layer remained. This second anneal was used to obtain desired band edge for the mirror and phase sections. The remaining implant buffer layer and 1.3Q stop etch layers were

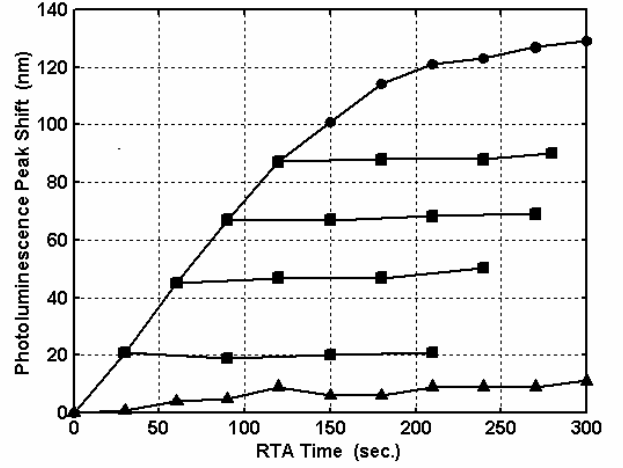


Fig. 3. Peak photoluminescence peak shift as a function of anneal time, showing the initial linear increase in the peak shift and the complete halting of the peak shift for samples for which the implant buffer layer has been etched. Symbols indicate nonimplanted (triangles), implanted (circles), and samples with partial anneal followed by the removal of the implant buffer layer (squares).

removed using a wet etch process, leaving a thin planar InP surface just above the waveguide. This gives access to the high field region of the optical mode, which is ideal for etching high coupling coefficient gratings, on the order of 300 cm^{-1} , directly into the waveguide. The remainder of the device process is described in detail in [8].

V. RESULTS

A. QWI

The intermixing process was calibrated using several samples cleaved from an implanted seven QW base structure, as described in the previous section. These samples were annealed at 675 $^\circ\text{C}$ for various times ranging from 30-seconds to 300-seconds at 30-second intervals and the extent of the intermixing was measured by room-temperature photoluminescence. As the vacancy front moves through the QW region the blue-shift increases linearly. Once the vacancy front has moved through the QW region, blue-shifting ceases. This saturation of the blue-shift can be observed above 120 nm as shown in Fig. 3. After the 30, 60, 90, 120-second anneals, the implant buffer layer was removed from the respective samples. These samples were then subjected to additional anneal cycles. We found that removing the implant buffer layer halted the blue-shift during these anneals. The arrest of the blue-shift is the result of the removal of the abundance of vacancies, necessary for intermixing, along with the implant buffer layer. We believe that the vacancies travel through the entire device structure to the n-type substrate, which acts as a vacancy sink, keeping the vacancies far from the active region. The uniformity of the intermixed QWs should be quite good, due to the fact that the vacancies travel through the entire active region. This is further supported by the fact that the full width at half maximum (FWHM) of the photoluminescence response does not increase post intermixing.

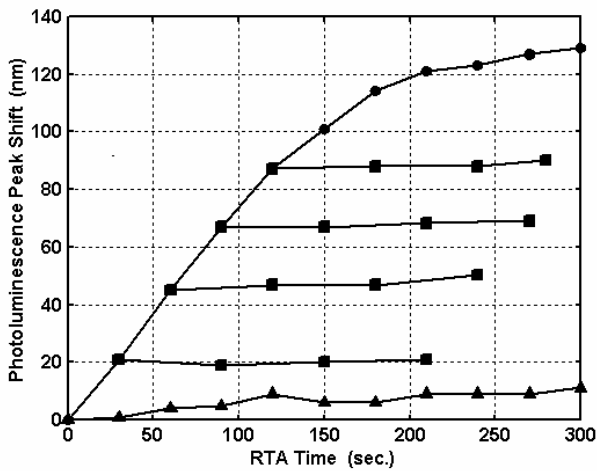


Fig. 4. Photoluminescence spectra for a ten-quantum well sample showing three band-edges achieved with a single ion implant. Symbols indicate active region photoluminescence (diamonds), EAM photoluminescence (squares), and mirror and phase section photoluminescence (triangles).

With this process, it is possible to achieve any number of band edges across the wafer, limited only by the practical number of lithographic process steps. For this paper, only three band-edges were needed, the as grown bandgap for the gain regions, a band-edge ideal for the mirror and phase tuning sections, and an intermediate band-edge for the EAM.

We found the quality of the QWI material in all three regions to be quite good as characterized by the peak intensity and FWHM of the photoluminescence curves. The photoluminescence curves for a ten QW sample, used in this work, are shown in Fig. 4.

B. Active/Passive Fabry-Perot Buried Ridge Structure (BRS) Lasers

An important parameter in the SGDBR device is the modal loss in the mirror and phase sections at the gain peak of the active region. Not only does the modal loss in these regions have a large effect on the untuned output power of the device, but also, plays a large role in determining the power ripple in the tuning band. Using active/passive devices, where the passive region is composed of intermixed QWs, the modal loss of the intermixed QWs used in the mirror and phase sections can be extracted. This is done by plotting the differential efficiency of the active/passive device as a function of passive region length. The method is described in [8]. Fig. 5 shows the experimental data with the theoretical fit for regions shifted to the band-edge for both the tuning and EAM sections. The tuning and EAM region modal loss was computed to be 1.5 cm^{-1} and 6.4 cm^{-1} , respectively.

The loss due to the passive region band edge was investigated by testing active/passive lasers that possessed differing magnitudes of intermixing in the passive region. The passive region loss was plotted as a function of photoluminescence peak wavelength for both seven and ten QW active regions, shown in Fig. 6. An exponential curve fit was applied to the seven QW active region data, while the ten QW active region data is fit to the same curve with the addition of a constant term. As evident from the figure, the

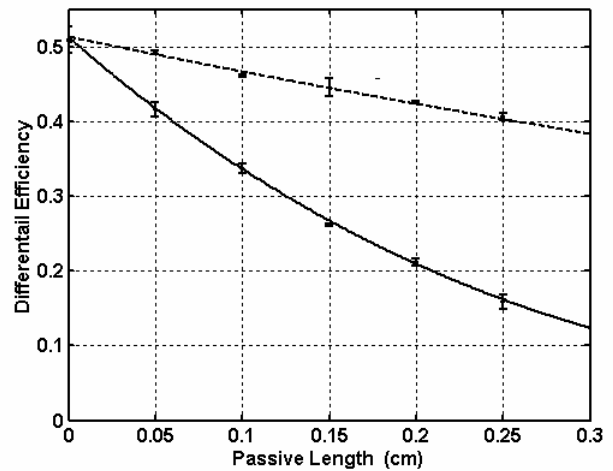
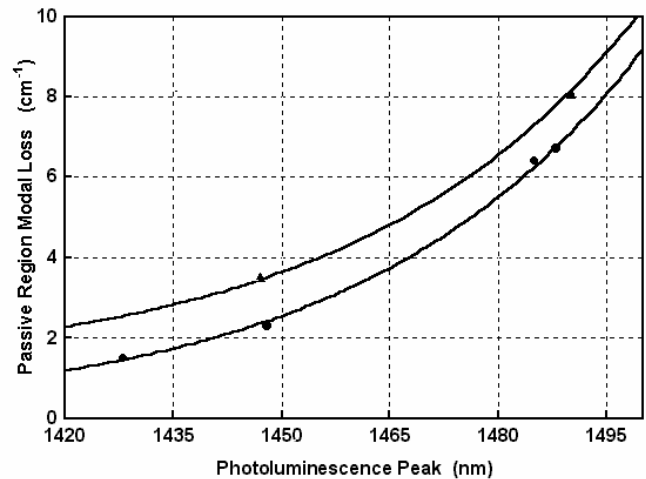


Fig. 5. Extraction of passive region modal loss by plotting differential efficiency of active/passive devices as a function of passive region length for both the mirror band edge (dotted line), and the EAM band edge (solid line). Modal loss values were computed to be 1.5 cm^{-1} and 6.4 cm^{-1} , for the mirror band edge and EAM band edge, respectively.



passive region modal loss is strongly dependent on the relative position of the intermixed band edge.

C. Carrier Induced Tuning

The extent of intermixing also affects the maximum tuning range. In order to determine the affect of the extent of intermixing on the tuning range, three samples with differing amounts of intermixing were tested for the tuning range. The SG-DBR lasers were processed along with the active/passive lasers presented in the previous section. This way the maximum achievable tuning range can be plotted as a function of peak wavelength shift and related to the modal loss in the tuning region. The tuning curves for the samples are shown in Fig. 7. From the figure, the sample with the intermediate band edge has the greatest tuning range, while the sample with the least amount of intermixing also tunes the least.

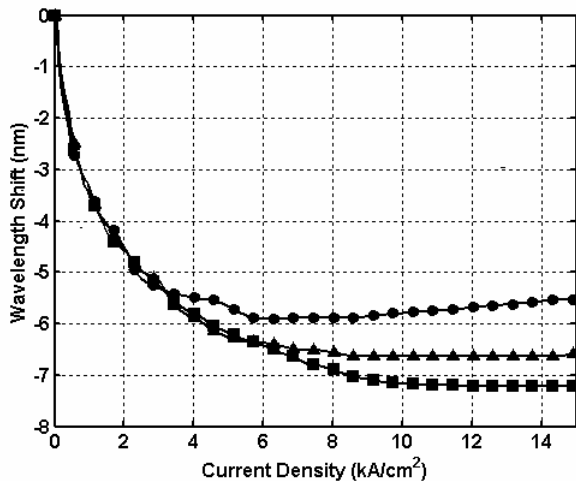


Fig. 7. Experimental tuning curve for samples with differing extents of intermixing. Symbols indicate wavelength shifts of 1475 nm (circles), 1446 nm (squares), and 1423 nm (triangles).

TABLE I
SUMMARY OF MODAL LOSS AND TUNING
RANGE FOR INTERMIXED QWS

| Number QWs | Bandgap λ (nm) | $\langle\alpha_i\rangle$ (cm^{-1}) | $\Delta\lambda_{\text{tune}}$ (nm) |
|------------|------------------------|---|------------------------------------|
| 7 | 1428 | 1.5 | 6.6 |
| 7 | 1448 | 2.3 | 7.2 |
| 7 | 1485 | 6.4 | 5.9 |
| 10 | 1447 | 3.5 | 8.0 |

Using the tuning range versus peak wavelength shift, and the modal loss versus peak wavelength shift, the optimal placement of the band edge can be determined. It is advantageous to minimize the modal loss while maximizing the tuning in the SG-DBR mirror. In this case, the maximum separation occurs at a photoluminescence peak wavelength shift in the vicinity of 1430 nm. Table 1 summarizes the modal loss and tuning values with respect to the photoluminescence peak wavelength for both seven QW and ten QW devices. The ten QW sample has a 1.2 cm^{-1} greater modal loss and 0.8 nm greater tuning than a seven QW sample with a similar band edge. It may be advantageous to make use of a larger number of QWs in the tuning region, increasing the available tuning, and allowing the mirror to be designed with a smaller sampling period, thus reducing the overall length of the mirror, and possibly the loss through the mirror.

D. SGDBR Laser

The SG-DBR lasers demonstrate excellent characteristics in terms of output power, threshold current, and SMSR. Both seven and ten QW active region devices were fabricated and tested. The seven QW devices exhibited lower threshold

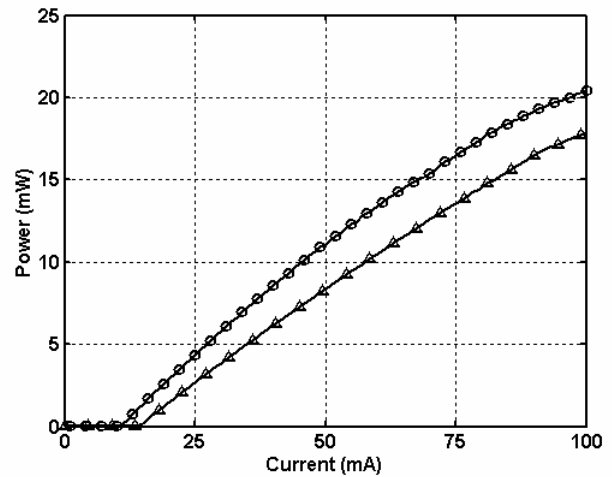


Fig. 8. Typical output power versus current for seven (circles) and ten (triangle) quantum well devices. The mirror design used in these devices consisted of a peak wavelength spacing of 7 nm, burst lengths of 6 nm and 5 nm, 12 and 4 periods, for the back and front mirror, respectively.

current and slightly higher slope efficiency due to the lower magnitude of optical loss present in the device. The current versus light output for these devices is shown in Fig. 8. The output power for both the seven and ten QW devices reached over 20 mW, while the threshold current was 11 mA and 14 mA for the seven and ten QW devices, respectively. The SMSR for the typical SG-DBR device fabricated with this process is 40 dB or greater. These characteristics match well with the simulations for this mirror design.

E. EAM Extinction and Bandwidth

The modulator bandgap was placed 50 nm blue shifted from the peak gain wavelength. This location will allow for a low insertion loss, yet is close enough that a significant increase in absorption can be obtained with reverse bias. A photoluminescence peak wavelength scan is shown in Fig 9, showing three band edges, with the modulator band edge placed at around 1500 nm.

The extinction characteristics for modulators with several lengths and either seven or ten QW absorption regions are presented in this section. The modulators were tested for several wavelengths using the integrated SG-DBR laser. As expected, the extinction varied for the different input wavelengths with the best extinction occurring at the shortest wavelength. The length of the modulator had the effect of improving the extinction with increasing length. The extinction of the ten QW device proved to possess a much larger extinction for all wavelengths over the seven QW device. The extinction curves of a 225 μm long seven QW device are shown in Fig.10 for various wavelengths. The onset of absorption occurs at around -1 V , with extinction reaching 5 dB for a wavelength of 1580 nm and 22 dB for a wavelength of 1540 nm at a reverse bias of 7 V. The magnitude of the extinction increases with length of the modulator as shown in Fig. 11, where 125 μm and 225 μm long devices are compared.

The devices using ten QWs had a much greater extinction ratio than did the seven QW devices. The extinction curves of

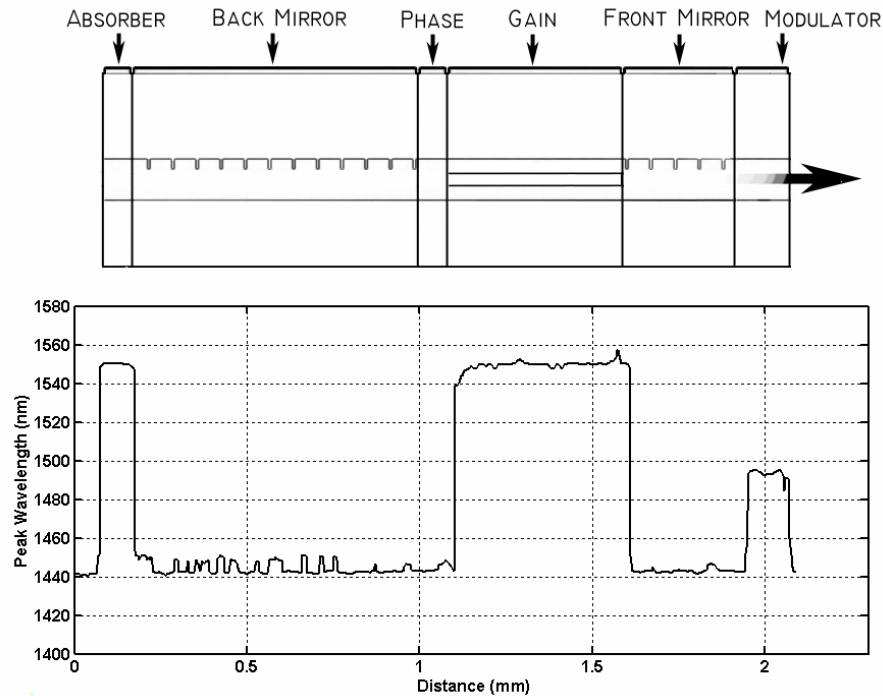


Fig. 9. Typical photoluminescence peak wavelength scan of SG-DBR device with integrated EAM. Device layout is shown above for reference.

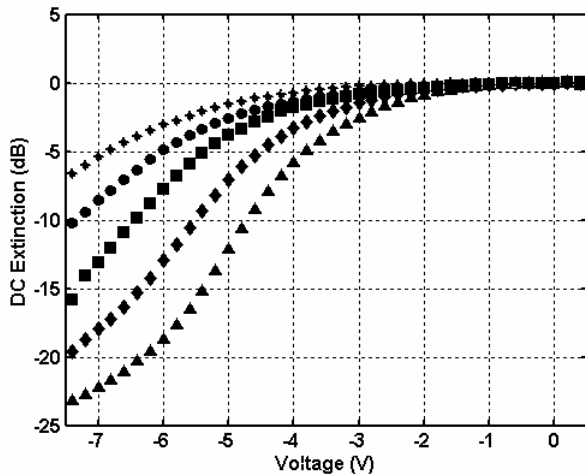


Fig. 10. DC extinction of a seven quantum well absorption region with a length of 225 μm for various wavelengths. Symbols indicate wavelengths of 1580 nm (stars), 1570 nm (circles), 1560 nm (squares), 1550 nm (diamonds), and 1540 nm (triangles).

a ten QW device are shown in Fig. 12. These 125 μm long devices achieve extinction ratios between 10 dB and 22 dB for wavelengths of 1585 nm and 1555 nm, respectively. In fact, the extinction of the ten QW devices achieve around 10 dB more extinction than a seven QW device with the same length. This coupled with the fact that the SG-DBR performance is only slightly reduced for the ten QW device suggests that it is advantageous to use a greater number of QWs in the base structure growth. Thus, enabling the use of a shorter

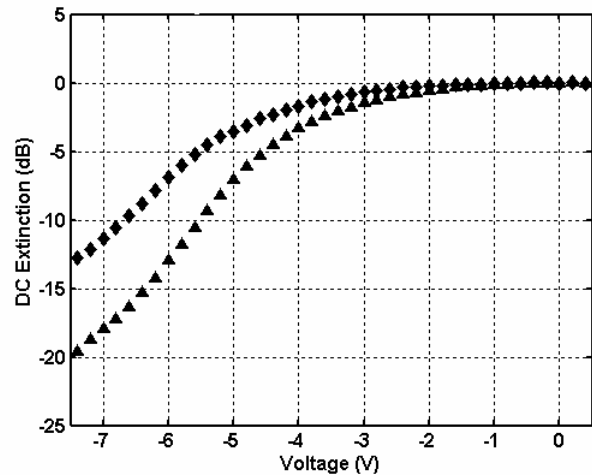


Fig. 11. DC extinction of devices with a seven quantum well absorption region for various lengths. Symbols indicate modulator device lengths of 125 μm (diamonds), and 225 μm (triangles).

modulator section, which serves to reduce the capacitance and improve the bandwidth.

The devices were subject to bandwidth measurements using a lightwave component analyzer. The devices exhibited 3 dB bandwidths ranging from 7.5 to 9.0 GHz, limited by capacitance. The longer devices, 225 μm , possess the most capacitance limiting the 3 dB bandwidth. The bandwidth measurements for the seven QW devices are shown in Fig. 13. The bandwidth of these devices can be improved by reducing the length, as indicated by the figure, but in doing so the extinction properties suffer, as described above.

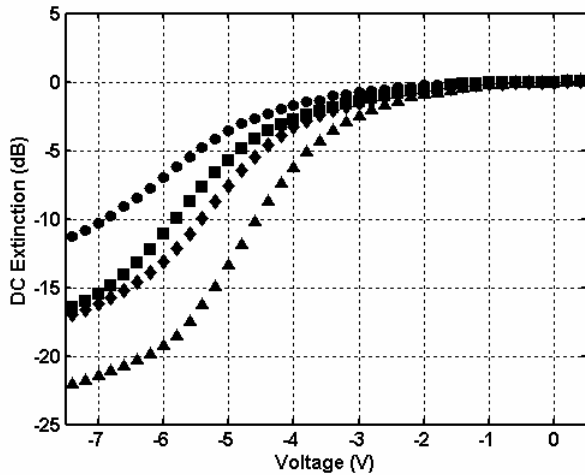


Fig. 12. DC extinction of a ten-QW absorption region with a length of 125 μm for various wavelengths. Symbols indicate wavelengths of 1585 nm (circles), 1575 nm (squares), 1565 nm (diamonds), and 1555 nm (triangles).

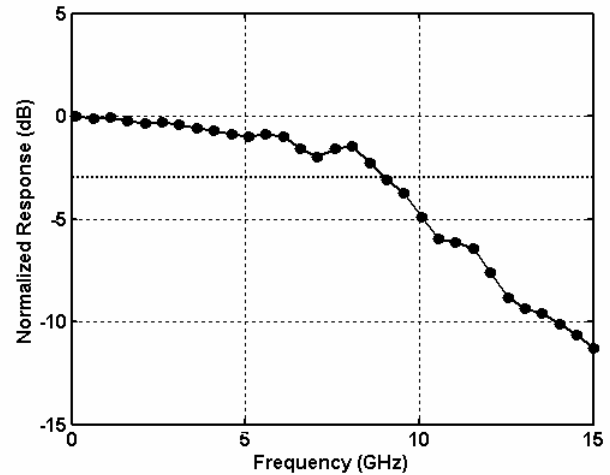


Fig. 14. Bandwidth measurement for a ten-QW device at a length of 125 μm . A 3 dB bandwidth of 9.0 GHz was observed.

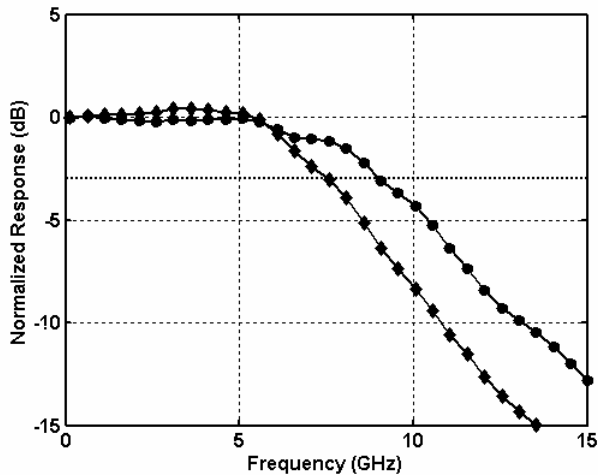


Fig. 13. Bandwidth measurements for seven-QW devices. Symbols indicate modulator lengths of 125 μm (circles), and 225 μm (triangles). The 3 dB bandwidths were 7.5 GHz and 9.0 GHz for lengths of 225 μm and 125 μm , respectively.

One solution would be to use a ten QW absorption region, which exhibits a larger extinction than seven QW devices, allowing the length of the device to be reduced, while maintaining an acceptable extinction ratio. The 3 dB bandwidth measurements are shown in Fig. 14, were a bandwidth of 9.0 GHz was achieved.

VI. CONCLUSION

We have employed a quantum well intermixing process, using a single ion implant, in the fabrication of widely tunable SGDBR lasers with integrated EAMs. An implant buffer layer is used to capture an ion implant, producing vacancies far from the active region. A rapid thermal process is used to partially diffuse the vacancies through the multiple-QW active region. Once the desired extent of intermixing has been observed, the implant buffer layer is removed. Doing so

removes the source of vacancies above that particular region, effectively halting the intermixing process, freezing the band edge. Further anneals continue to intermix in regions where the implant buffer layer remains. The anneal/etch process can be cycled a number of times allowing any number of unique band edges.

Widely tunable SG-DBR lasers were characterized in terms of threshold current, output power, and SMSR. The SG-DBR lasers performed exceptionally well in all respects. The threshold currents were on the order of 10 to 15 mA, while the output power reached upwards of 20 mW, while the SMSR proved to be sufficient at 40 dB or greater. The monolithically integrated EAM possessed a band edge intermediate to that of the gain and mirror sections. Modulators based on seven and ten QW absorption regions were characterized. The extinction increased with increasing length and number of QWs. The bandwidths of the modulators were measured for several lengths indicating limitations due to capacitance.

It is important to note that the QWI process described is general in its application and can be used to monolithically integrate a number of devices each with a unique band edge.

REFERENCES

- [1] J. Binsma, P. Thijs, T. VanDongen, E. Jansen, A. Staring, G. VanDenHoven, and L. Tiemeijer, "Characterization of Butt-Joint InGaAsP Waveguides and Their Application to 1310 nm DBR-Type MQW Ganin-Clamped Semiconductor Optical Amplifiers," *IEICE Trans. Electron.*, vol. E80-C, pp. 675-681, May 1997.
- [2] M. Aoki, M. Suzuki, H. Sano, T. Kawano, T. Ido, T. Taniwatari, K. Uomi, and A. Takai, "InGaAs/InGaAsP MQW Electroabsorption Modulator Integrated with a DFB Laser Fabricated by Band-Gap Energy Control Selective Area MOCVD," *IEEE J Quantum Electron.*, vol. 29, pp. 2088-2096, June 1993.
- [3] B. Mason, J. Barton, G. Fish, and L. Coldren, "Design of Sampled Grating DBR Lasers with Integrated Semiconductor Optical Amplifiers," *IEEE Photon. Technol. Lett.*, vol. 12, pp. 762-764, July 2000.
- [4] B. Mason, G. Fish, S. DenBaars, and L. Coldren, "Widely Tunable Sampled Grating DBR Lasers with Integrated Electroabsorption Modulator," *IEEE Photon. Technol. Lett.*, vol. 11, pp. 638-640, June 1999.

- [5] B. Mason, S. DenBaars, and L. Coldren, "Tunable Sampled-Grating DBR lasers with Integrated Wavelength Monitors," *IEEE Photon. Technol. Lett.*, vol. 10, pp. 1085-1087, August 1998.
- [6] Y. Akulova, G. Fish, P. Koh, C. Schow, P. Kozodoy, A. Dahl, S. Nakagawa, M. Larson, M. Mack, T. Strand, C. Coldren, E. Hegblom, S. Penniman, T. Wipiejewski, and L. Coldren, "Widely Tunable Electroabsorption-Modulated Sampled-Grating DBR Laser Transmitter," *IEEE J. Sel. Topics in Quantum Electron.*, vol. 8, pp. 1349-1357, November/December 2002.
- [7] S. Charbonneau, E. Kotels, P. Poole, J. He, G. Aers, J. Haysom, M. Buchanan, Y. Feng, A. Delage, F. Yang, M. Davies, R. Goldberg, P. Piva, and I. Mitchell, "Photonic Integrated Circuits Fabricated Using Ion Implantation," *IEEE J. Sel. Topics in Quantum Electron.*, vol. 4, pp. 772-793, July/August 1998.
- [8] E. Skogen, J. Barton, S. DenBaars, and L. Coldren, "A Quantum-Well-Intermixing Process for Wavelength-Agile Photonic Integrated Circuits," *IEEE J. Sel. Topics in Quantum Electron.*, vol. 8, pp. 863-869, July/August 2002.
- [9] V. Jayaraman, Z. Chuang, and L. Coldren, "Theory, Design, and Performance of Extended Tuning Range Semiconductor Lasers with Sampled Gratings," *IEEE J. Quantum Electron.*, vol. 29, pp. 1824-1834, June 1993.
- [10] E. Li, and W. Choy, "Electro-Absorptive Properties of Interdiffused InGaAP/InP Quantum Wells," *J. Appl. Phys.*, vol. 82, pp. 3861-3869, October 1997
- [11] M. Paquette, V. Aimez, J. Beauvais, J. Beerens, P. Poole, S. Charbonneau, and A. Roth, "Blueshifting of InGaAsP-InP Laser Diodes Using a Low-Energy Ion-Implantation Technique: Comparison Between Strained and Lattice-Matched Quantum-QW Structures," *IEEE J. Sel. Topics in Quantum Electron.*, vol. 4, pp. 741-745, July/August 1998.